Green-function theory of scanning tunneling microscopy: Tunnel current and current density for clean metal surfaces

G. Doyen, D. Drakova,* and M. Scheffler
Fritz-Haber-Institut der Max-Planck-Gesellschaft, Faradayweg 4-6, D-14195 Berlin, Germany
(Received 27 December 1991; revised manuscript received 4 August 1992)

A theory of scanning tunneling microscopy (STM) is presented that accounts for a realistic treatment of the electronic structure of the sample surface. The sample is represented by a semi-infinite crystal built from muffin-tin potentials describing the atomic structure and surface electronic wave functions of *s*, *p*, *d*, etc., electrons. The other electrode carrying the tip atom is a planar free-electron metal surface. The potential of the tip atom is expanded in a localized basis set. Within the single-particle approach, the exact equation for the scattering wave for the combined system (tip plus sample) is derived. It is evaluated using a Green-function technique. From the scattering wave function the spatial distribution of the current density is obtained. The method is applied to study the tunnel current to clean Al(111), Pd(111), and Pd(100) surfaces. At typical tip-sample separations (≥ 3 Å) the substrate atoms appear as protrusions. Quite remarkable, the contrast is found to be larger in the Al(111) images than in the Pd(111) and Pd(100) images. This is a consequence of the tip-sample interaction. As a further consequence of tip-sample interactions we find that at *close* distances between the tip and the Pd surfaces the *interstitial regions* appear as maxima in the variation of the tunnel current. The theory covers a broad range of tip-sample separations, including those where perturbation treatments of STM theory (as, e.g., developed by Tersoff and Hamann) break down. A systematic analysis of the different aspects that may affect the tunnel current is presented.

I. INTRODUCTION

To date, an unambiguous interpretation of atomic-resolution surface topography, as obtained by scanning tunneling microscopy, does not exist. This is particularly so for metal surfaces, where typically no localized (dangling-orbital-like) wave functions exist. The importance of an improved understanding of scanning tunneling microscopy (STM) becomes apparent for STM from adsorbates. Here it is now well established experimentally that adatoms do not always show up as protrusions in the contours of constant tunnel current,[1] contrary to what might be expected from simple local electron-density arguments.[2] Nevertheless, in the interpretation of STM images of clean metal surfaces it is nearly always assumed that the protrusions represent metal atoms. A justification of this assumption does not exist. In fact, we will show below that under certain conditions this assumption is incorrect.

Several three-dimensional approaches to the theory of STM have been formulated,[3–7] which do not rely on Bardeen's perturbation approach,[14] but still apply one or another approximation. In particular, a proper description of the scattering behavior of the tunneling electrons in the sample is missing in many theories. Our approach concentrates on a realistic description of the sample surface and takes multiple scattering of the electrons in the sample and between the sample surface and the tip into account.

In this paper we illustrate some interesting features of the STM tunneling process using simple model potentials for the barrier and the tip. It sheds some light on the problem of imaging surface atoms and investigates the conditions under which they might appear as indentations or protrusions. The theory has predictive power, if realistic potentials are used.

Scanning tunneling microscopy has repeatedly obtained atomic resolution on a number of clean and adsorbate-covered metal surfaces.[8–11] Some *sp*-type metal surfaces (having no or only little *d*-electron density at the Fermi level) were found to show a particularly large contrast of the STM images compared to transition-metal surfaces. A rather unexpected observation is, for example, the large corrugation amplitude on atomically and electronically flat surfaces of *sp* metals, such as Al(111) (Ref. 11) or Au(111).[8] In the case of Au(111), due to the very low *d*-electron density at the Fermi energy, a more or less *sp*-metal behavior is expected, which classifies the imaging of Au(111), as well as Al(111), as a difficult problem of STM theory. Our investigation may contribute towards a possible physical explanation of the large corrugation on *sp*-metal surfaces. In experiment, the STM corrugation amplitude does not only depend on the tip-sample separation, but also on the atomic structure and composition of the tip which frequently changes in an uncontrolled manner. Physical effects of a special nature (tip instabilities, resonance tunneling) might be responsible for an anomalously large corrugation obtained by means of a special preparation of the tip. These aspects are not addressed in the present investigation. We model a rather simple and rigid tip which should simulate tips obtained without special preparation. We shall compare the imaging of an *sp*-metal surface [Al(111)] with the imaging of transition-metal surfaces [Pd(111) and Pd(100)] and explain the differences in physical terms.

Section II describes the formalism to evaluate the tunnel current and outlines the evaluation of the scattering

wave function from which the current density is obtained. It also defines the quantities tip-projected local density (TIP-LOD) and capacitor-projected local density (CAP-LOD), which we find helpful in the interpretation of the numerical results. Section III defines the model for the sample and the tip. Sections IV and V present the results for the different sample surfaces and Sec. VI gives a comparative discussion.

II. SCATTERING THEORY OF STM

In this section we describe the basic formalism of our STM theory. Expressions for the tunnel current and the scattering wave function are derived and the quantities CAP-LOD and TIP-LOD are defined, which allow us to quantify the influence of the tip-sample interaction on the tunnel current, and therefore are essential for the interpretation of the numerical results.

A. General theory

The task of a theory of scanning tunneling microscopy is to calculate the current flowing from the tip to the sample surface or vice versa depending on the applied voltage. In a single-particle picture this can be viewed as a scattering process where, e.g., an electron incident from the interior of the tip metal scatters at the barrier and has a certain probability of penetrating into the sample surface. The total Hamiltonian has the form

$$H = H^0 + V^{\text{tip}} , \tag{1}$$

$$H^0 = -\frac{\hbar^2 \Delta}{2m_e} + V^{\text{cap}} . \tag{2}$$

H^0 is the Hamiltonian of a two-electrode system (capacitor) without tip atom (cf. Fig. 1), m_e is the electron mass, V^{cap} is the potential of the capacitor which includes the barrier potential and the potential inside the two electrodes, and V^{tip} is the potential induced by a tip atom, which would break any spatial symmetry that might exist for the two-electrode system. The voltage applied between tip and sample in STM experiments is included in the theory by shifting the inner potentials on the tip and sample sides so that the difference of the Fermi energies ΔE equals the electron charge e times the applied voltage. The bias is chosen such that the current flows from the

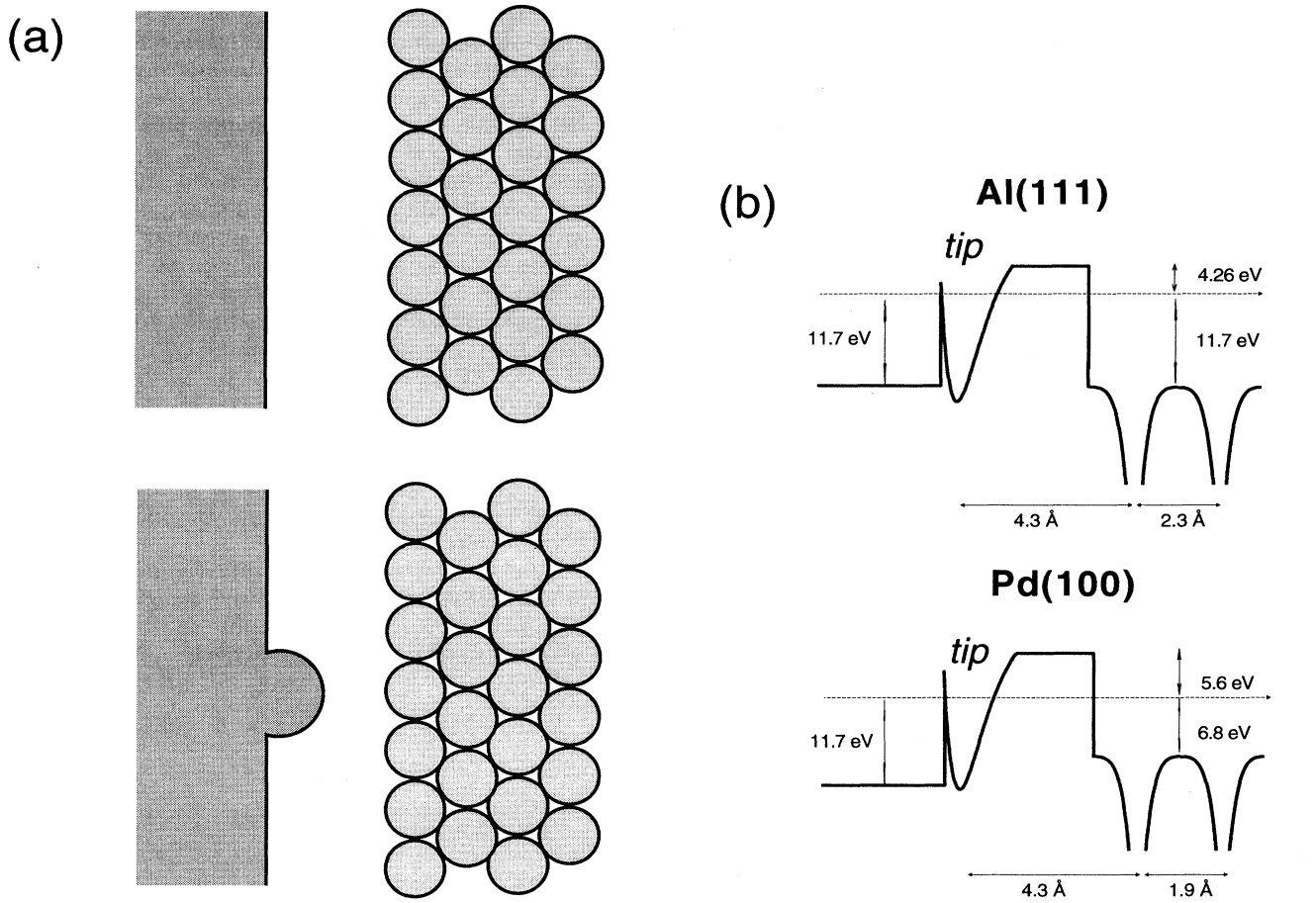

FIG. 1. Schematic representation of the potential for the model STM consisting of a half-infinite muffin-tin sample (right) and a free-electron electrode with a model tip. (a) Upper half: Two-electrode system (capacitor) having parallel translational invariance. Lower half: Tip atom included. (b) A cut along the normal to the Al(111) and Pd(100) surfaces through the tip atom center.

tip to the sample, i.e., we have electron waves incident from the bulk of the tip towards the sample.

The current itself is the electron charge e times the number of electrons which tunnel per unit time. According to Lippmann's generalization[12] of Ehrenfest's theorem[13] the tunnel current can be written in the following form:

$$J=2\frac{\pi e}{\hbar}\sum_{f,i}|\langle \mathbf{f}_{\rm cap}|V^{\rm tip}|\mathbf{i}+\rangle|^2\delta(E_f-E_i)\ . \tag{3}$$

Within the single-particle picture this expression is exact. The sum runs over all states with energy between the two Fermi levels having the correct scattering boundary conditions. The scattering process is described by a wave function $|\mathbf{i}+\rangle$ which is an eigenfunction of the total Hamiltonian including the tip potential $V^{\rm tip}$. $\mathbf{i}$ indicates the incoming momentum of the electron inside the tip electrode. When measuring the current, the scattered electron with final outgoing momentum $\mathbf{f}$ (after the electron has passed through the sample) is detected in the wave function $|\mathbf{f}_{\rm cap}\rangle$, which does not experience the potential $V^{\rm tip}$ in the barrier region. This means that $|\mathbf{f}_{\rm cap}\rangle$ has to be an eigenstate of the Hamiltonian H^0 satisfying outgoing scattering boundary conditions, i.e., it has to describe a Bloch state propagating away from the interface with scattered wave components collapsing towards the scattering centers,

$$|\mathbf{f}_{\rm cap}\rangle=(1+G^{\rm cap,-}V^{\rm cap})|\mathbf{f}\rangle\ , \tag{4}$$

$|\mathbf{f}\rangle$ is a plane wave. Within the present formalism the scattering experienced by the incoming electrons due to the tip and sample potentials is fully taken into account. The perturbing potential $V^{\rm tip}$ is localized in coordinate space and can be expanded in a set of functions $|A\rangle$ which are localized near the tip atom in the barrier region. Using a nonorthogonal expansion set we obtain

$$V^{\rm tip}=\sum_{A,B,C,D}|A\rangle S^{-1}_{AB}\langle B|V^{\rm tip}|C\rangle S^{-1}_{CD}\langle D|\ . \tag{5}$$

S^{-1}_{AB} is a matrix element of the inverse overlap operator in the localized basis.

Introducing the above expansion of $V^{\rm tip}$ into Eq. (3) then yields an expression for the tunnel current which contains quantities that are easily accessible to physical interpretation. If we consider the limit where the applied voltage $\Delta E/e$ tends to zero, we get

$$J=\lim_{\Delta E\to 0}\frac{2\pi e}{\hbar}\frac{1}{\Delta E}\sum_{A,B,C,D,}\mathcal{S}^{\rm tip}_{AB}\mathcal{S}^{\rm cap}_{CD}\tilde{V}_{BC}\tilde{V}_{DA} \tag{6}$$

with

$$\mathcal{S}^{\rm tip}_{AB}=\sum_i\langle A|\mathbf{i}+\rangle\langle\mathbf{i}+|B\rangle\ , \tag{7}$$

$$\mathcal{S}^{\rm cap}_{CD}=\sum_f{}^{\rm capacitor}\langle C|\mathbf{f}_{\rm cap}\rangle\langle\mathbf{f}_{\rm cap}|D\rangle\ . \tag{8}$$

In this section the scattering states are considered as generalized eigenvectors with δ-function normalization. The summations in Eqs. (7) and (8) should in general run over states in the energy range between the two Fermi levels. In the limit $\Delta E\to 0$ the summations run over states on the energy shell. Using the δ-function normalization J, $\mathcal{S}^{\rm tip}_{AB}$ and $\mathcal{S}^{\rm cap}_{CD}$ then tend to zero, but the ratio $eJ/\Delta E$, which is the tunnel conductivity, tends to a finite value. $\tilde{V}_{BC}$ is a matrix element of the operator

$$S^{-1}V^{\rm tip}S^{-1}=\sum_{A,B,C,D}|B\rangle S^{-1}_{BA}\langle A|V^{\rm tip}|D\rangle S^{-1}_{DC}\langle C|\ . \tag{9}$$

$\mathcal{S}^{\rm tip}_{AB}$ is a matrix element of the projection operator $\sum_i|\mathbf{i}+\rangle\langle\mathbf{i}+|$ in the localized basis set. The projection is on the eigenfunctions of the total Hamiltonian with boundary conditions corresponding to incident waves from the tip side. $\mathcal{S}^{\rm tip}_{AA}$ is the projection of the local function $|A\rangle$ in the barrier on those exact scattering eigenstates that are generated by incident waves running towards the sample surface and will be termed *tip-projected local density* (TIP-LOD).

$\mathcal{S}^{\rm cap}_{AB}$ is the corresponding projection on the eigenstates of the system without the tip atom, which resembles a capacitor of two plane electrodes. These are eigenfunctions of H^0 with boundary conditions corresponding to Bloch waves $|\mathbf{f}_{\rm cap}\rangle$ propagating away from the interface. The diagonal matrix elements represent the electron density of the corresponding wave functions at the Fermi level averaged over the tip region. $\mathcal{S}^{\rm cap}_{AA}$ is the projection of the local state on eigenfunctions of the two-electrode system without tip atom and is called *capacitor-projected local density* (CAP-LOD). It may be interpreted as a partial local charge density at the Fermi level of the unperturbed two-electrode system (sample plus free-electron electrode).

The set of functions $\{|A\rangle\}$ localized in the barrier is chosen to define the tip region and shape, i.e., the region in position space, where the tip potential acts. Hence, the meaning of the capacitor and tip-projected local electron densities is just the electron density at the Fermi level projected onto the region, where the tip potential is effective for the system without and with tip. The CAP-LOD's include information about the electron structure of the sample, whereas the additional information gained from TIP-LOD's can be attributed to the tip-sample interaction. This means that the comparison of the tunnel current contrast with the variations of CAP-LOD and TIP-LOD yields information about the influence of tip-sample interactions.

It might be tempting to substitute the quantities CAP-LOD and TIP-LOD by the negative imaginary parts of the Green function of the capacitor ($G^{\rm cap,+}$) and of the exact Green function (G^+), respectively,

$$-\frac{1}{\pi}{\rm Im}G^{\rm cap,+}_{AA}(E_F)=\sum_k\langle a|\mathbf{k}\rangle\langle\mathbf{k}|A\rangle\delta(E_F-E_k)\ , \tag{10}$$

$$-\frac{1}{\pi}{\rm Im}G^{+}_{AA}(E_F)=\sum_k\langle A|\mathbf{k}+\rangle\langle\mathbf{k}+|A\rangle\delta(E_F-E_k)\ . \tag{11}$$

The important difference is that the summations in TIP-LOD and CAP-LOD, as defined by Eqs. (7) and (8), are not over a complete set of eigenfunctions on the energy

shell as they are for the imaginary parts of the respective Green functions.

In Bardeen's perturbation theory,[14] which is the basis of many state-of-the-art STM theories, the interaction of the tip and the tip electrode with the sample surface is neglected and $|\mathbf{f}_{\mathrm{cap}}\rangle$ and $|\mathbf{i}+\rangle$ are replaced by eigenfunctions of standing wave character $|\mathbf{k}_{\mathrm{sample}}\rangle$ and $|\mathbf{k}_{\mathrm{tip}}\rangle$ of the noninteracting sample and tip, respectively. As a consequence of this approximation, the generalized Ehrenfest theorem reduces to Fermi's golden rule and $\mathcal{S}^{\mathrm{tip}}_{AA}$ does not vary with lateral tip position. In this limit S^{cap}_{AA} is reduced to S^{sample}_{AA} and the current would be proportional to

$$\mathcal{S}^{\mathrm{sample}}_{AA}=\sum_{k}^{\mathrm{sample}}\langle A|\mathbf{k}_{\mathrm{sample}}\rangle\langle\mathbf{k}_{\mathrm{sample}}|A\rangle\ . \tag{12}$$

S^{sample}_{AA} is the local charge density at E_F of the unperturbed sample, described by wave functions $\{|\mathbf{k}_{\mathrm{sample}}\rangle\}$, averaged over the tip orbital $|A\rangle$. It is termed *sample-projected local density* (SAP-LOD). For an s-type tip orbital $|A\rangle$ at sufficiently large distance from the sample surface this represents essentially the Tersoff-Hamann approximation.[2]

B. Numerical procedure

The most difficult part of a STM theory which attempts to accurately evaluate Eq. (3) is the calculation of the scattering wave function $|\mathbf{i}+\rangle$. In our approach a Green-function technique is applied to evaluate $|\mathbf{i}+\rangle$ and to calculate the current without applying perturbation theory. The tip breaks any spatial symmetry by introducing the local perturbation V^{tip} representing the tip potential. The Lippmann-Schwinger equation is used to calculate the exact scattering wave function

$$|\mathbf{i}+\rangle=|\mathbf{i}_{\mathrm{cap}}\rangle+G^{\mathrm{cap},+}V^{\mathrm{tip}}|\mathbf{i}+\rangle\ . \tag{13}$$

$|\mathbf{i}_{\mathrm{cap}}\rangle$ and $G^{\mathrm{cap},+}$ are the eigenfunction and the Green operator for the two-dimensionally translational invariant system without tip, respectively,

$$|\mathbf{i}_{\mathrm{cap}}\rangle=(1+G^{\mathrm{cap}+}V^{\mathrm{cap}})|\mathbf{i}\rangle\ . \tag{14}$$

V^{tip} is restricted to the region around the tip atom which is spanned by the localized basis set $\{|A\rangle\}$. The projection of the exact scattering state on the localized basis is then obtained by

$$\langle A|\mathbf{i}+\rangle=\langle A|\mathbf{i}_{\mathrm{cap}}\rangle+\sum_{B,C,D,F}\langle A|G^{\mathrm{cap},+}|C\rangle S^{-1}_{CD}V^{\mathrm{tip}}_{DF}S^{-1}_{FB}\langle B|\mathbf{i}+\rangle\ . \tag{15}$$

This equation is useful, if the solution of the two-electrode system is known and if the perturbing potential is limited to a small area in space as is the case for the tip. Solving explicitly for the wave function, we need to perform a matrix inversion. The size of the matrix depends on the basis set. Matrix inversion is only necessary in the subspace $\{|A\rangle\}$, where the tip-induced potential is nonzero,

$$\langle A|\mathbf{i}+\rangle=\sum_{B}(1-G^{\mathrm{cap},+}V^{\mathrm{tip}})^{-1}_{AB}\langle B|\mathbf{i}_{\mathrm{cap}}\rangle\ . \tag{16}$$

Outside the localized area defined by the tip, the wave function can be obtained by a simple matrix multiplication.[6]

In the present implementation of the theory, Eqs. (15) and (16) provide the scattering wave function in the barrier as an expansion of the form

$$\psi_i(\mathbf{r})=\langle\mathbf{r}|\mathbf{i}+\rangle=\sum_{\mathbf{k}}\langle\mathbf{r}|\mathbf{k}\rangle\langle\mathbf{k}|\mathbf{i}+\rangle\ , \tag{17}$$

where $\{|\mathbf{k}\rangle\}$ represents a complete set of basis states consisting of plane waves parallel to the surface and exponentials in the perpendicular direction. The summation is again on the energy shell $E_{\mathbf{k}}=E_F$. Equation (17) is used to evaluate the current density of this state according to the well-known formula

$$\mathbf{j}(\mathbf{r})=\frac{e\hbar}{m_e}\,\mathrm{Im}(\psi_i^*(\mathbf{r})\nabla\psi_i(\mathbf{r}))\ . \tag{18}$$

If the current density is integrated over a plane parallel to the surface, the total current for the considered scattering state $|\mathbf{i}+\rangle$ is obtained. It is this quantity which is calculated in this work for a normalization of $\psi_i(\mathbf{r})$ corresponding to an incident wave $e^{i\mathbf{k}\mathbf{r}}$. With this normalization the integral of $\mathbf{j}(\mathbf{r})$ is nonzero. We refer to this quantity in the following as the "tunnel current." Summing Eq. (18) over all possible incident waves yields then a result which is equivalent to Eq. (3).[15] The results obtained in such a way can be interpreted by means of Eq. (6), which contains quantities helpful for a qualitative understanding.

III. DEFINITION OF THE MODEL

In the detailed calculations which we describe below, we start from the equations described in Sec. II and use them together with a model system which is schematically illustrated in Fig. 1: The semi-infinite crystal is built from muffin-tin potentials taken from self-consistent bulk calculations.[16] Our method would allow us to use different potentials at the surface atom layers as, for example, obtained from self-consistent slab calculations. Although individual wave functions are modified significantly at the surface, the potentials are only little affected. This holds at least for close-packed, unreconstructed metal surfaces. We therefore use the same potentials at the surface layers as for the bulk. We confirmed that the electron density of states at the surface is practically indistinguishable from that obtained by self-consistent full-potential slab calculations.

In order to have parallel translational invariance for $G^{\mathrm{cap},+}$, the potential in the interior of the tip metal is kept constant which means that the tip base is represented by a free-electron metal. The work function and the energetic width of the occupied free-electron states are chosen to correspond to Al(111) ($\phi_{\mathrm{Al(111)}}=4.26$ eV, $V_0=11.68$ eV, $r_s=2.07$ bohr). The region of flat potential inside the tip electrode is separated from the semi-infinite sample by a square barrier, which is positioned at the rim of the first layer muffin-tin spheres.

In the next step of the calculation a localized attractive potential is introduced, which should model the tip. As the microscopic structure of the tip is unknown, we decided for the present study to assume the following shape, which is computationally convenient. The tip potential is defined as

$$V^{\mathrm{tip}} = V^{\mathrm{loc}} | A \rangle \langle A | , \tag{19}$$

where $| A \rangle$ is a normalized function centered in front of the tip electrode with a Gaussian shape parallel to the surface. Perpendicular to the surface it is a Gaussian cutoff at the rectangular barrier. V^{loc} is a constant. In the following we shall refer to the localized potential V^{tip} and the localized function $| A \rangle$ describing it as the "tip atom."

We consider in the present investigation only tunneling electrons with kinetic energy at the Fermi level. This means that the voltage is taken such that the Fermi levels of the two electrodes are at the same energy. The incident momentum is perpendicular to the electrode surfaces. As a consequence, there is no summation over incident waves and no quantitative values for the magnitude of the tunnel current are therefore given below. For this special choice the TIP-LOD and CAP-LOD are the following:

$$\mathcal{S}^{\mathrm{tip}}_{AA} = \langle A | \mathrm{i}+ \rangle \langle \mathrm{i}+ | A \rangle ,$$

$$\mathcal{S}^{\mathrm{cap}}_{AA} = \sum_{f}^{\text{capacitor}} \langle A | \mathrm{f}_{\mathrm{cap}} \rangle \langle \mathrm{f}_{\mathrm{cap}} | A \rangle ,$$

and the tunnel current is proportional to $\mathcal{S}^{\mathrm{tip}}_{AA} \mathcal{S}^{\mathrm{cap}}_{AA} (V^{\mathrm{loc}})^2$ [cf. Eqs. (6)–(8)]. In order to obtain nonzero values, TIP-LOD and CAP-LOD are evaluated with an appropriate normalization of the wave functions (cf. Sec. II B).

The Green functions $G^{\mathrm{cap},\pm}$ which are needed to evaluate Eqs. (4) and (16) and which describe a system consisting of two electrodes (capacitor) are calculated by a layer Korringa-Kohn-Rostoker (KKR) scheme developed by Kambe, Scheffler, and Maca.[17,18] Parallel translational invariance allows the application of Bloch's theorem to expand the wave function and the Green operator in reciprocal space. The evaluation of the matrix elements $G^{\mathrm{cap},\pm}_{AA}$ requires then an integration over the surface Brillouin zone. This integration and the evaluation of the current density are the time determining steps in the calculations.

IV. TUNNEL CURRENT TO AN Al(111) SURFACE

The muffin-tin potentials for the Al atoms are taken from the self-consistent bulk calculations of Moruzzi, Janak, and Williams.[16] The Fermi level is at 11.68 eV relative to the muffin-tin zero. The work function is 4.26 eV (Ref. 21) so that for the two-electrode system (capacitor) the barrier height as seen from the sample side is 15.94 eV relative to the muffin-tin zero. The kinetic energy of the tunneling electron is 11.68 eV.

The Gaussian representing the tip atom is centered at 1.1 Å in front of the tip electrode and has a lateral radial range of ~ 1.7 Å parallel to the surface (decay $\alpha = 0.1$ bohr^{-2}). The expectation value of the local tip potential in the region of the Gaussian is $V^{\mathrm{loc}} = -13.6$ eV.

A. Tunnel current and local charge densities at the Fermi level

Figure 2 shows a slight periodic change in the total tunnel current when the tip is moved parallel to the surface at a constant perpendicular separation of 3.5 Å of the center of the tip from the first layer of Al atoms. The calculated STM image of Al(111) in Fig. 2 is typical at this and larger tip-sample separations, except for the different corrugation amplitudes at different perpendicular distances. The relative variation of the total tip-induced current is $\sim 5.5 \times 10^{-12}$ at 3.5 Å. The current is enhanced, when the tip is above an Al atom, which is in accordance with the experimental findings.[1,11] However, the absolute magnitude of the theoretically predicted variation is too small compared to the experiments by Wintterlin *et al.*[11] Experimentally, corrugations on Al(111) varying between 0.1 and 0.8 Å have been reported dependent upon tip-sample distance, which in terms of tunnel currents means relative variations of the order of 50% or larger. The microscopic structure of the tip and its chemical composition as well as the quantum mechanics of the large tunnel current variation are still a matter of debate. In order to address this question additional calculations are needed, which compare different tip atoms.

The local tip Green function G^{+}_{AA}, which is a matrix element of the Green operator G^{+}, is plotted in Fig. 3 as a function of energy for a tip-sample separation of 4.3 Å.

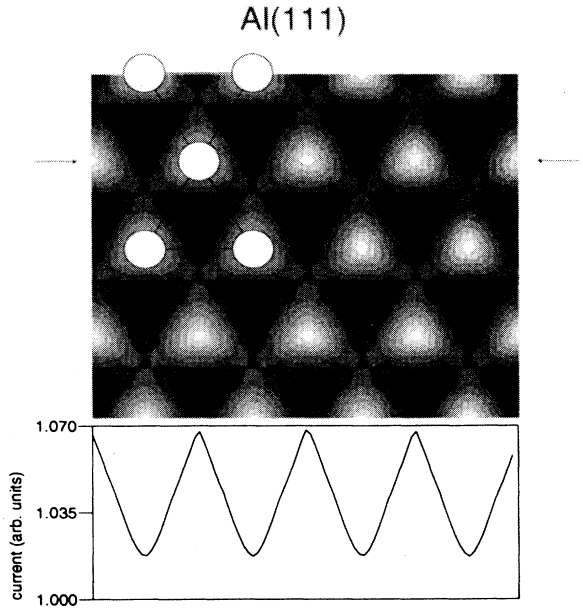

FIG. 2. Variation of the total tunnel current parallel to an Al(111) surface for a tip-sample separation of 3.5 Å. The maximal variation is 5.5%. The empty circles indicate Al atoms in the first layer.

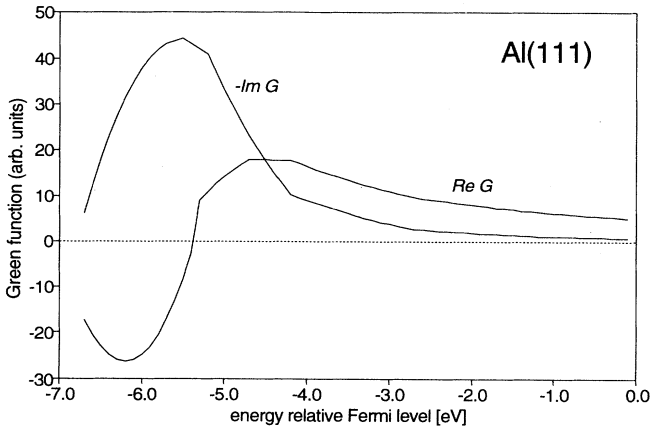

FIG. 3. Energy dependence of $-\mathrm{Im}G^{+}_{AA}$ at a tip-sample separation of 4.3 Å with the tip above an Al atom.

It exhibits a peak at approximately 5.5 eV below the Fermi level which implies a resonance induced by the local tip potential. The value of the imaginary part of this tip Green function at the Fermi level is roughly proportional to the TIP-LOD, although we have to remember that $\mathcal{S}^{\mathrm{tip}}_{AA}$ is *not* identical to $-(1/\pi)\,\mathrm{Im}G^{+}_{AA}(E_F)$, because the summation in TIP-LOD as required by Eq. (7) is not over a complete set of eigenfunctions on the energy shell. However, a *tip-induced* variation of the tunnel current parallel to the surface due to tip-sample interaction would imply a concurrent variation of $-(1/\pi)\,\mathrm{Im}G^{+}_{AA}(E_F)$ and of TIP-LOD. The results show that the corrugation of these quantities is small but follows qualitatively that of $\mathcal{S}^{\mathrm{cap}}_{AA}$ (CAP-LOD) which is shown in Fig. 4. Hence the lateral variation of the current has the same shape as the charge density at the Fermi level without tip-sample interaction, but the amplitude is somewhat larger.

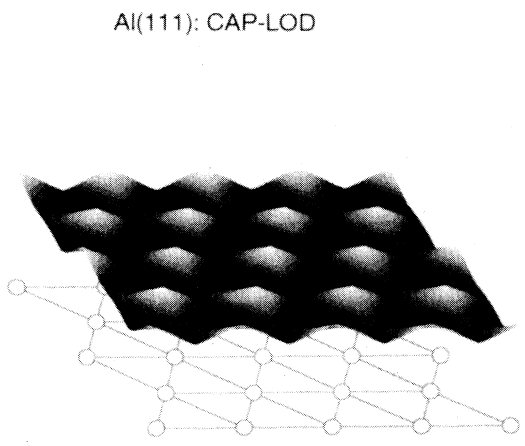

FIG. 4. Lateral variation of the capacitor projected local density at the Fermi level (CAP-LOD) [cf. Eq. (8)] for Al(111) at a tip-sample separation of 4.3 Å.

Results with this kind of STM theory for Al(111) have been published before.[20] However, in this earlier work we used a different barrier position, a different value of V^{loc}, and a tip-sample separation corresponding to contact situation. The variations of the tunnel current were even smaller than in the present calculation and exhibited tiny maxima for the tip over the hollow position. These different results were due to a stronger influence of the TIP-LOD at smaller distances, which tends to increase the current to the interstitial region, and emphasize the possible importance of the barrier potential. The neglect of the image potential might also affect the quantitative aspects of the results. This will be investigated in a later publication.

V. TUNNEL CURRENT TO Pd(111) AND Pd(100) SURFACES

For the Pd sample we again use the self-consistent bulk potentials of Moruzzi, Janak, and Williams.[16] This gives a Fermi level at $V_0=6.8$ eV. Together with the work functions $\phi_{\mathrm{Pd}(100)}=5.6$ eV, $\phi_{\mathrm{Pd}(111)}=5.95$ eV (Ref. 21) we thus have that the barrier height on the sample side is now 12.4 eV on Pd(100) and 12.75 eV on Pd(111), the kinetic energy of the tunneling electron is 6.8 eV relative to the muffin-tin zero.

A. Tunnel current and local charge densities at the Fermi level

Palladium has a *d*-electron density at the Fermi level and therefore might be expected to exhibit a stronger variation of the charge density parallel to the surface than Al(111), which could be reflected in the tunnel current. Surprisingly, this is not the case at moderately large distances (4.3 Å), where we find a relative variation of the tunnel current of only 2.2% for the Pd surfaces with maxima above the atoms (cf. Fig. 5).

At smaller distances (1.8 Å) the situation changes and the tunnel current becomes maximal in the threefold hollow site (fcc site) on Pd(111) and in the fourfold hollow position on Pd(100) with a decrease of 2.5% on shifting from the hollow to the top position. We shall see below that this is an influence of the *d* electrons and is in contrast to the situation for Al(111). Figures 6 and 7 demonstrate that this is, however, not a property of the isolated Pd surfaces, because the CAP-LOD's show maxima above the atoms even for small separations.

In order to analyze the situation we plot in Figs. 6 and 7 the CAP-LOD's and the TIP-LOD's for the two considered tip-sample separations on Pd(100), since the two Pd surfaces show very similar behavior. The behavior of the TIP-LOD changes qualitatively at small separations [cf. Fig. 7(b)] and reflects the trends displayed by the tunnel current. The nature of this tip-sample interaction becomes clear from Fig. 8, where the energy dependence of the negative imaginary parts of the translationally invariant Green function [Eq. (10)] and the Green function of the system with the tip atom [Eq. (11)] are plotted for barrier width 1.6 Å and tip-sample separation 1.8 Å. The values of $-\mathrm{Im}G^{\mathrm{cap},+}_{AA}(E_F)$ and $-\mathrm{Im}G^{+}_{AA}(E_F)$ as a function of the tip position are roughly parallel to those of

CAP-LOD and TIP-LOD, respectively. Figure 8(b) displays, in addition to $-\mathrm{Im}G_{AA}^{\mathrm{cap},+}$ of Pd(100), the spectral resolution of the negative imaginary part of the Green function $-\mathrm{Im}G_{AA}^{+}$ of a structureless jellium sample for the same tip and barrier as we use for Pd(100). The energy position of the tip-induced resonance state is strongly distance dependent and shifts to higher energy as the barrier becomes narrower mainly due to increasing kinetic energy as a result of confining the variational space into a narrower barrier.

At small separations the interaction between the resonance state of the localized tip potential and the d states of Pd, which show up as structure in the imaginary part of $G_{AA}^{\mathrm{cap},+}$ between -1.5 and -3 eV below the Fermi level [cf. Fig. 8(a)], is so strong that splitting into bonding and antibonding states is observed. This is due to the

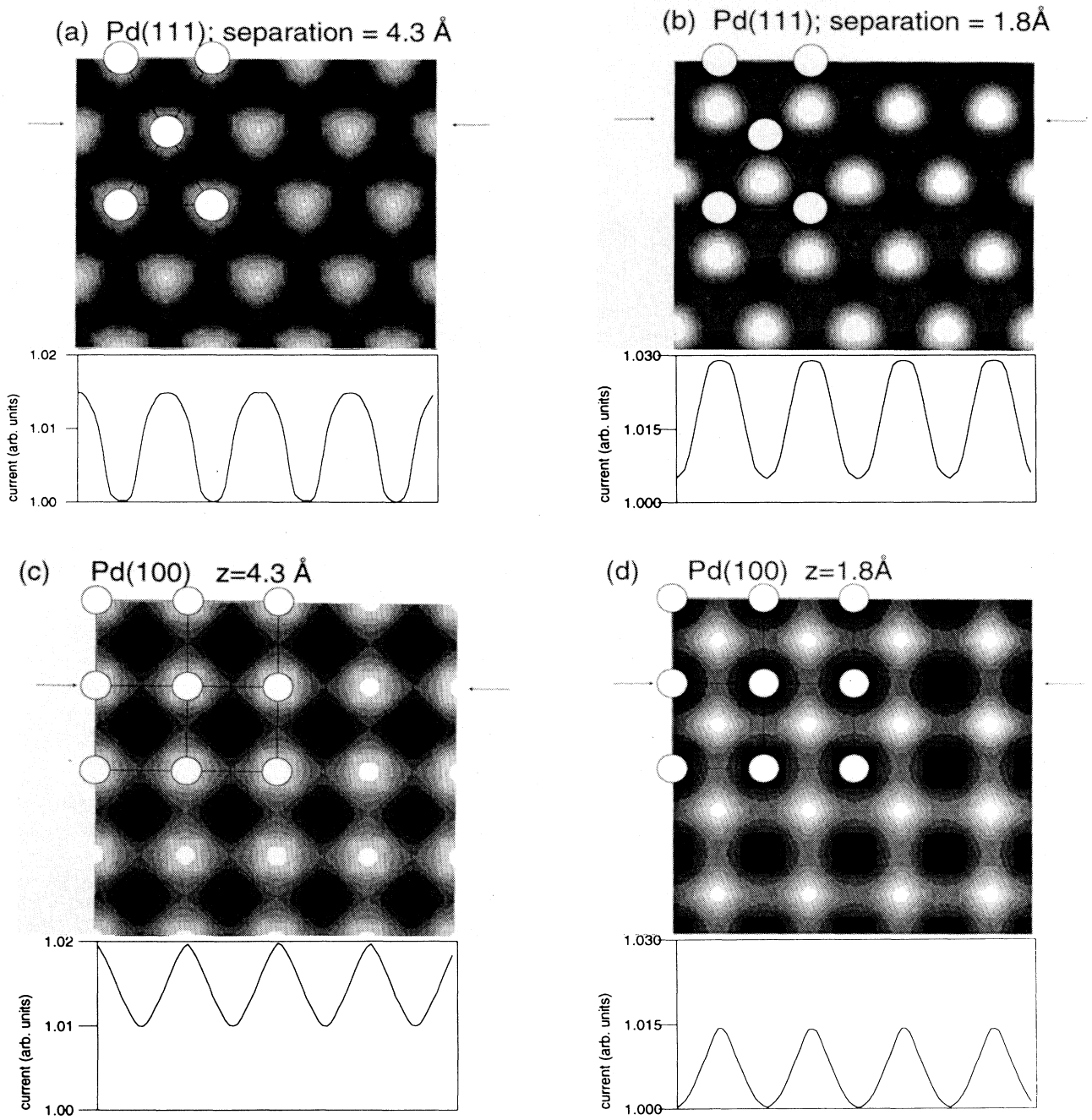

FIG. 5. Variation of the total tunnel current parallel to a Pd(111) and a Pd(100) surface at tip-sample separations of 4.3 [(a) and (c)] and 1.8 Å [(b) and (d)]. The open circles indicate the positions of the Pd atoms in the first layer.

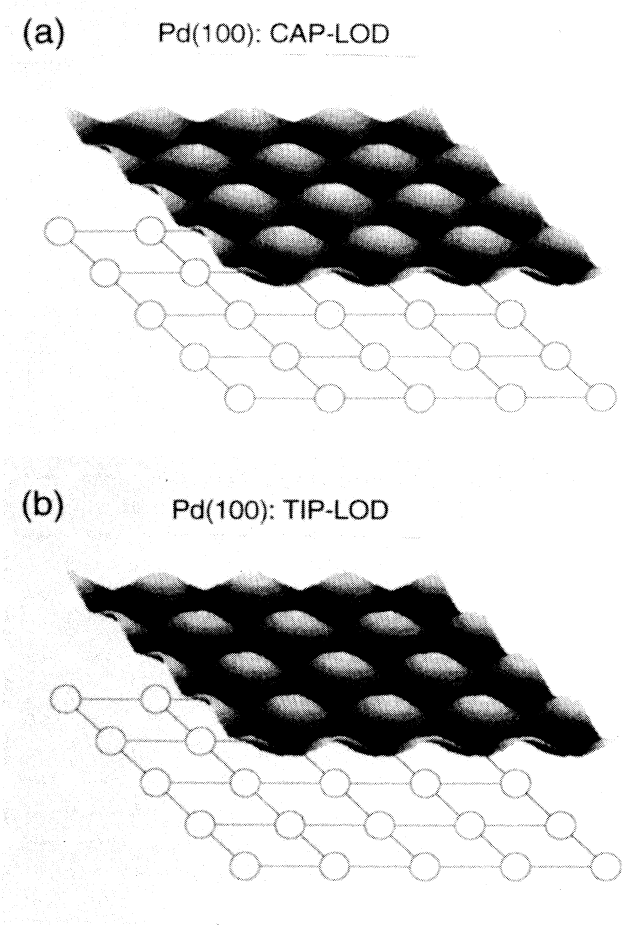

FIG. 6. Lateral variation of CAP-LOD (a) and TIP-LOD (b) for Pd(100) [cf. Eqs. (8) and (9)] for a tip-sample separation of 4.3 Å.

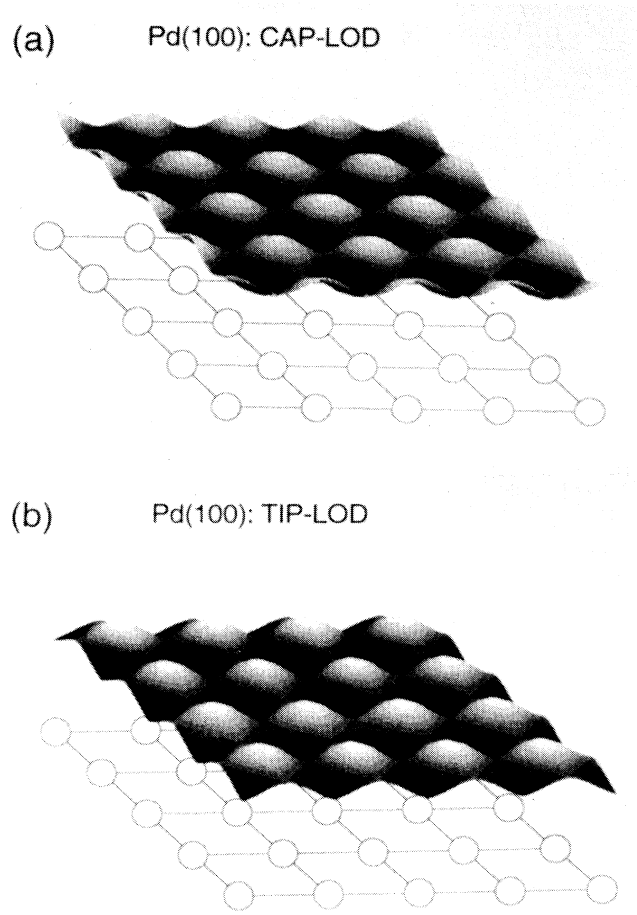

FIG. 7. Lateral variation of CAP-LOD (a) and TIP-LOD (b) for Pd(100) [cf. Eqs. (8) and (9)] for a tip-sample separation of 1.8 Å.

quasidegeneracy of the tip resonance unperturbed by the sample and the *d*-derived structure in the imaginary part of the local Green-function $G_{AA}^{\text{cap},+}$ for the Pd surface without tip [cf. Fig. 8(b)]. The interaction is stronger for the hollow position than for the top position so that the antibonding state splits up to higher energy for the hollow position than for the top position. Therefore, the value of $-\text{Im}G_{AA}^{+}$ at the Fermi level is larger for the hollow position. This tip-induced relative enhancement of the density of states at the Fermi level in the hollow positions is reflected in enhancement of the charge density and tunnel current from the interstitial position compared to the top position.

B. Current density distributions

The current density distributions in position space yield a further insight into the tunneling between tip and sample, revealing the focusing of the scattered beam by the tip. This might be useful for understanding the differences between tip-sample interactions and tunneling on *sp*- and *d*-metal surfaces. The current density distributions can also be used to visualize some differences between the crystal faces of the same metal, e.g., Pd(111) and Pd(100), which are not necessarily reflected in the total tunnel currents.

Figure 9 displays the variation of the perpendicular component of the current density in a plane parallel to the electrode surfaces. The plane is situated where the potential step of the barrier occurs near the sample surface. Figure 9(a) shows the results for a tip with a structureless sample and Fig. 9(b) for a two-electrode system (capacitor without tip) with Pd(100) and Pd(111) surfaces. In both calculations the same width of the square barrier (4.1 Å) was used.

For the tip with the structureless sample the current density is cylindrically symmetric with respect to an axis passing through the tip atom. The current densities for the capacitor with one Pd(100) or Pd(111) electrode clearly exhibit maxima at the positions of the Pd atoms. On Pd(100) even at the positions of the second layer of Pd atoms some enhancement of the current density perpendicular to the sample surface can be observed. The current densities for the tip plus Pd(100) and Pd(111)

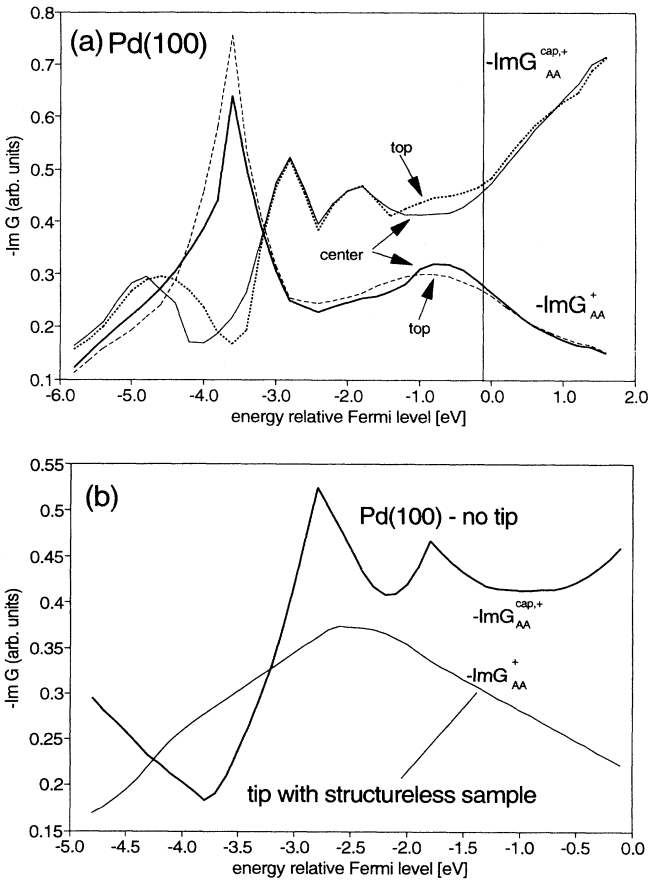

FIG. 8. Negative imaginary parts of the translational invariant Green-function $G_{AA}^{\mathrm{cap},+}$ [Eq. (8)] and the Green-function G_{AA}^{+} [Eq. (9)] for the system with tip atom: (a) for a Pd(100) sample at a tip-sample separation of 1.8 Å; (b) for a structureless sample surface with the same barrier width as in (a).

sample surfaces [displayed in Fig. 10(a), again with the same barrier width] arise from a superposition of the wave fields of the two situations of Fig. 9. The illuminating wave emanating from the tip and the scattered waves originating from the atoms in the sample form an interference pattern in a similar way as recently measured by low-energy electron holography.[22] The position of the Pd atoms is still discernible in the current density. For a tip plus an Al(111) sample surface this effect is less pronounced [cf. Fig. 10(b)].

Two factors have to be considered in order to explain these current density distributions: the attractive potential in the region of the tip atom and the barrier height. The influence of the attractive tip potential is schematically illustrated in Fig. 1(b). The different work functions of the investigated sample surfaces imply different tip potentials for the STM model defined in Sec. III. The work function is larger for the Pd surfaces than for Al(111) [for Pd(100) it is 5.6 eV, for Pd(111) 5.95 eV, and for Al(111) 4.26 eV]. Therefore in the case of Al(111) the tunneling electron experiences a more attractive potential when passing the tip atom. The electron beam should therefore be better focused in this case than in the case of Pd(100) and Pd(111). For the Pd surfaces the electron beam remains diffuse enough to be attracted by the adjacent Pd atoms. This spread of the tunneling current over a larger area is supported by the more attractive Pd muffin-tin potential (as compared to the Al potential) reflecting the influence of the *d* electrons. This correlates with a stronger tip-sample interaction as discussed above in terms of the TIP-LOD.

On the other hand a larger barrier height leads to a better focused electron beam as well. Hence, the barrier height, which is larger for the Pd samples than for Al(111), favors a better focused beam for Pd(100) and Pd(111) than for Al(111). The result of this competition (more attractive tip potential but smaller barrier height for Al) leads to a slightly better focused beam on Al(111).

The superimposed effect of tip attraction and different barrier heights for Pd(100) and Pd(111) can help to understand the differences between the two crystal faces. The barrier in front of Pd(100) is smaller and therefore more transparent, which explains why in the case of two plain electrodes the second-layer atoms are still visible in the current density for Pd(100) but not for Pd(111) [cf. Pd(111) and Pd(100) current densities in Fig. 9(b)]. Another reason why metal atoms are better resolved in the current density on Pd(100) than on Pd(111) is, of course, that the less dense packing of atoms on the (100) surface tends to decrease the current density in the interstitial regions.

The strong tip-sample interaction on Pd(111) and Pd(100) has consequences for the tunnel current images at closer distance [cf. the grey scale plots in Fig. 7(b)]. At close distance (1.8 Å) the tunnel current on both Pd surfaces is dominated by the tip-sample interaction through the TIP-LOD. On Pd(111) the tunnel current acquires a maximal value with the tip positioned above the fcc threefold hollow site where the tip-sample interaction is strongest. In the hcp position where the tip-sample interaction is weaker the tunnel current has a minimum. On Pd(100), on the other hand, the highest tunnel current is obtained in the center of the unit cell above an atom in the second layer as already discussed in detail in Sec. V A.

In this section we have been discussing fine details in the current density distributions in position space and this is not an observable quantity in STM. However, it proves helpful in illuminating some effects of the tip-sample interaction and probably in the future might gain more significance as an observable quantity in electron holography.[22]

VI. COMPARATIVE DISCUSSION OF THE RESULTS FOR THE SURFACES OF THE TWO METALS

At small tip Al(111) separations (1.8 Å) we observe a strong tip-sample interaction, but the change in the tunnel current still shows relative maxima on top and the variation from fcc hollow position to top amounts to 5.6%. We should point out that this distance is probably small compared to the normal tunneling distances in experiment and corresponds rather to point contact. Nev-

ertheless, we find that the effects at this small distance, which we shall identify below, play a role already at larger tip-sample separations and influence the STM image. The relatively small variation of the tunneling current at 1.8 Å originates from the counterbalancing influences of TIP-LOD and CAP-LOD. TIP-LOD shows an anticorrugating effect, because the tip-sample interaction is stronger in the hollow position where the tip atom interacts with more Al atoms than in the top position. However, the corrugating effect of CAP-LOD is not overcompensated by this behavior of TIP-LOD, it is only reduced. The small calculated corrugation cannot explain the experimental findings where in the constant current mode a corrugation of up to 0.8 Å has been observed.[11] The effects are small in the present theory, because the atomic Al potential has a weak scattering power. Ciraci, Baratoff, and Batra investigated this situation without calculating the tunnel current.[19] They found

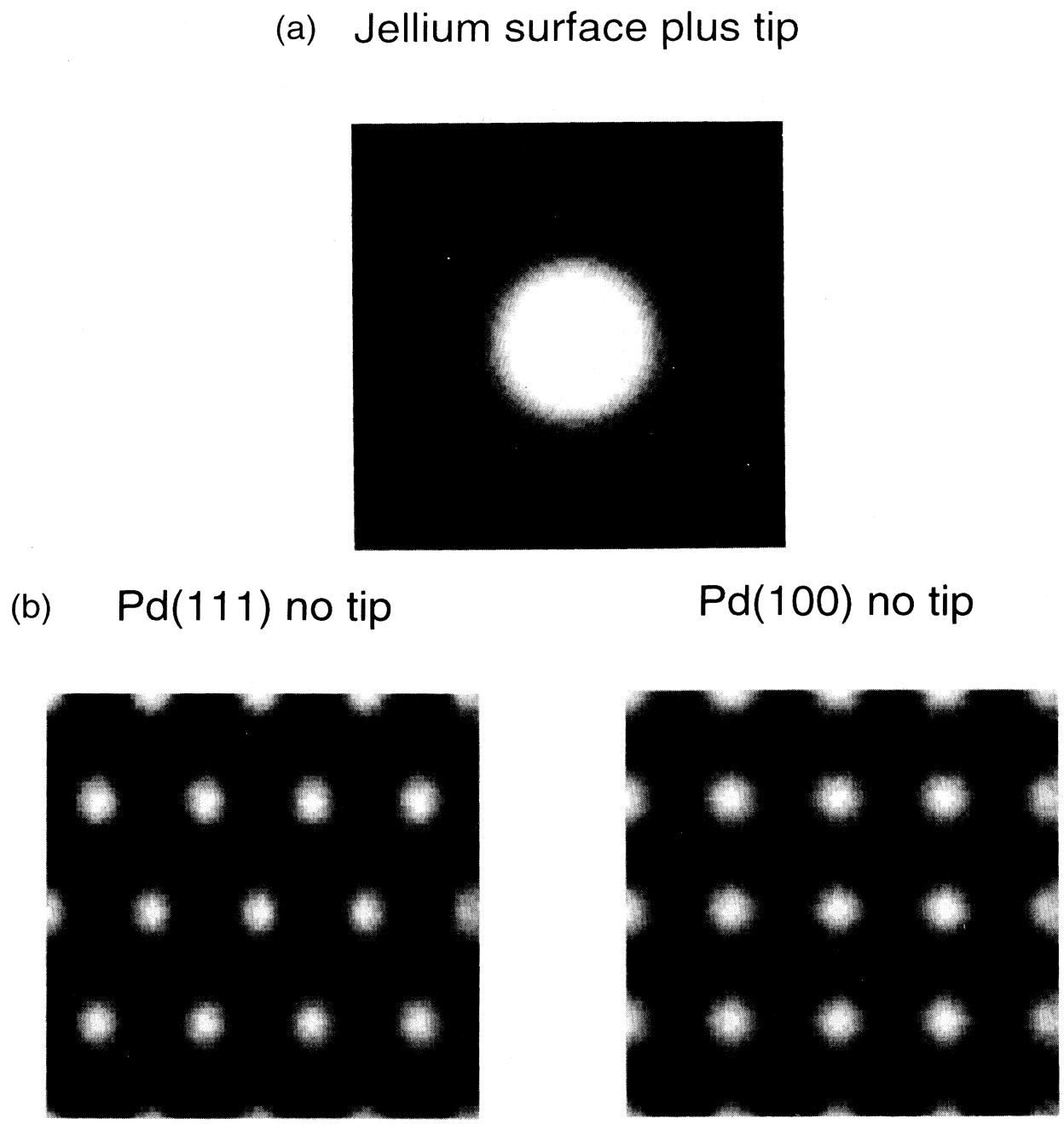

FIG. 9. Current densities for (a) tip with a structureless sample, (b) two electrode system (capacitor without tip) with Pd(100) and Pd(111) surfaces. The barrier width is the same in both cases (4.1 Å).

tip-induced localized states, which they suggested as explanation for anomalously large corrugation. Our calculations demonstrate that just because of the strong tip-sample interaction at short distances the variations of the tunnel current turn out to be small. This is at variance with the suggestion of Ciraci, Baratoff, and Batra.[19]

The *d* electrons on the Pd surfaces have a bearing on the tunnel current, if the tip atom is close enough to the sample surface so that covalent interactions play some role. The chemical bond formation increases the density of states at the Fermi level, because the antibonding state has some spectral weight here (cf. Fig. 8), and therefore leads to a larger tunnel current. The bond is somewhat stronger in the hollow position compared to the top position, because the tip atom "sees" more Pd atoms. This is reflected in the current density distribution in that the area illuminated by the electron beam is larger in the hollow position.

The effects of chemical bond formation between the tip atom and the sample surface are present for the Al(111)

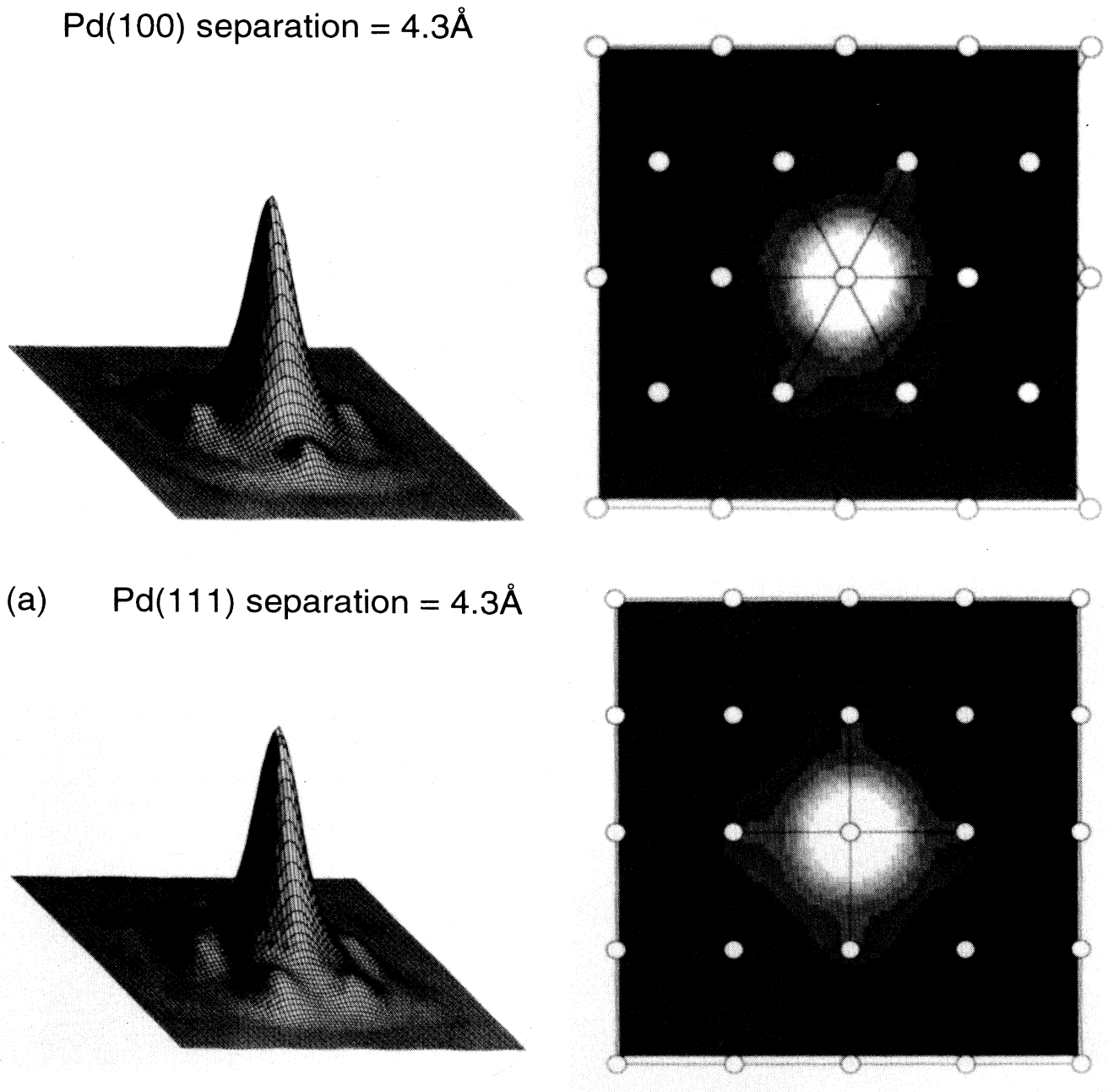

FIG. 10. 3D and Grey scale representation of the current density distribution parallel to the electrodes for the tip over a sample atom (tip-sample separation equal to 4.3 Å): (a) Pd(111) and Pd(100), (b) Al(111).

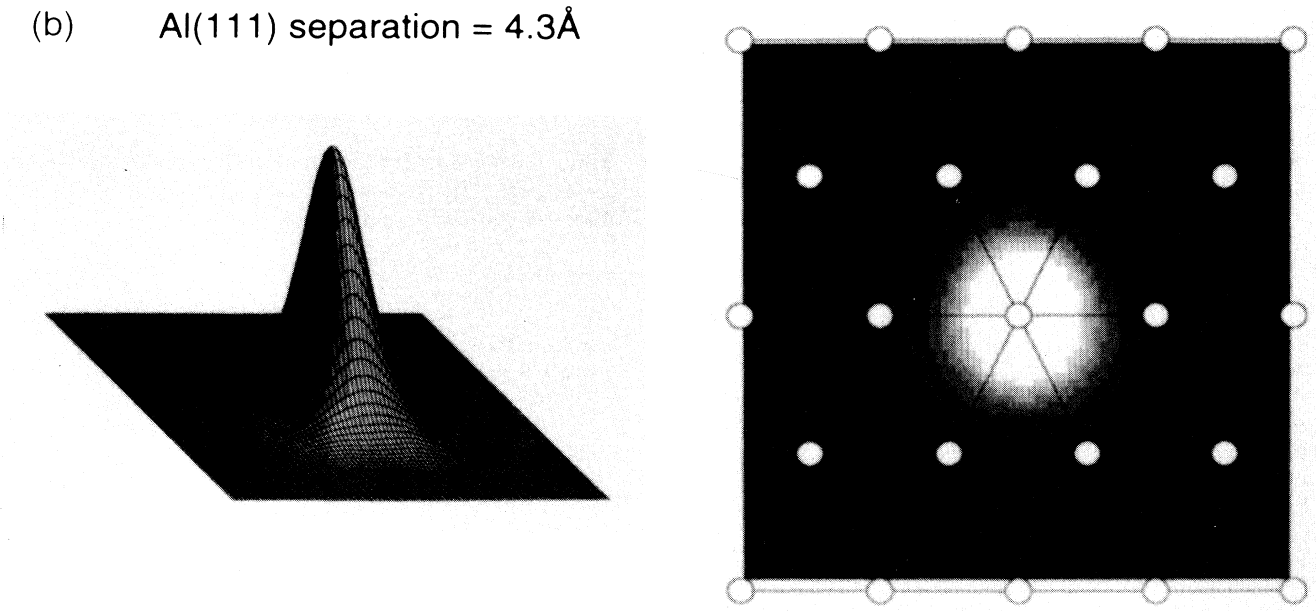

FIG. 10. (*Continued*).

surface as well, but they are smaller, because no d electrons are present which are nearly degenerate with the tip-induced resonance in the case of the paladium surfaces (cf. Fig. 8). Figure 10 demonstrates that for the tip position over an Al atom the current density distribution has a hexagonal shape. For top position on the Pd surfaces the current density distributions reflect the geometry of the sample surfaces in a quite pronounced way. The focusing effect for Al(111) mentioned above and the lack of the d electrons both act to suppress the influence of the atomic structure of the sample on the current density distribution.

Table I summarizes the results for the variation of the total tunnel current compared to the variation of the local charge density at the Fermi level. The latter quantity has been evaluated as the imaginary part of the Green-function matrix element $-\mathrm{Im}G_{AA}^{\mathrm{cap},+}$ for a contracted Gaussian (exponent $\alpha=10$ bohr^{-2}) at the tip center at different lateral positions relative to the sample.

At distances larger than 5 Å for Pd and 7 Å for Al the variation of the total tunnel current is equal to the variation of the local charge density of the metal surfaces. At somewhat smaller separations (4.5 Å) the tip-sample interaction acts on Pd to diminish the variations in the tunnel current relative to the charge-density variations, whereas on Al(111) the variations of the tunnel current are enhanced compared to the charge density. At very close separations (1.8 Å) the tip-sample interaction diminishes the corrugation on both metal surfaces.

TABLE I. Variation of total tunnel current and charge density at the Fermi level at the tip position (in brackets) between top and fcc hollow sites. Positive values indicate maximum on top site.

Tip-sample separation (Å)	Al(111)	Pd(111)	Pd(100)
1.8	5.6% (38%)	−2.5% (42%)	−2.5% (39%)
4.5	4.5% (3%)	2.2% (4%)	2.2% (3%)
6	1.2% (0.8%)	0.7% (0.7%)	0.8% (0.8%)
8	0.2% (0.2%)	0.1% (0.1%)	0.2% (0.2%)

The apparent paradoxical consequence of the described behavior is that the contrast in the total current variation is larger on Al(111) than on the Pd surfaces. This results from the fact that the chemical bond formation reflected in the TIP-LOD's, which is weaker for Al(111), has an anticorrugating effect and tends to enhance the tunnel current at tip positions of higher coordination.

VII. CONCLUSIONS

We have presented a KKR scattering theoretical approach to STM combined with a simple model for the tip. The theory leads in a natural way to the definition of the two quantities TIP-LOD and CAP-LOD, which directly enter in the calculation of the tunnel current and represent partial local charge densities characterizing the influence of the tip and sample side, respectively. The interpretation of these quantities offers insight into the physical nature of the tunneling process and demonstrates that the tip-sample interaction might have a qualitative bearing on the imaging properties. The physics is, however, somewhat more complex than suggested by Ciraci, Baratoff, and Batra in their discussion of tip-induced states.[19] For all investigated sample surfaces it tends to increase the tunnel current in the interstitial regions and therefore it may even lead to an inversion of the image, i.e., it may change the appearance of surface atoms from protrusions in the contours of constant tunnel current to indentations. A remarkable consequence

of this behavior is that at all investigated distances the atomic corrugation is larger on Al(111) than on Pd surfaces. These findings might be of importance for an explanation of the large corrugation seen in an experimental STM investigation of Al(111).[11]

Additional understanding is gained from the current density distributions in position space, which, e.g., illustrate the focusing effect of the tip. The described approach will be extended in the future to include a better description of the tip and the barrier potential.

ACKNOWLEDGMENTS

Financial support by the Sonderschungsbereich 6 is acknowledged. The authors are grateful to R. J. Behm and E. Koetter for useful discussions.

*Permanent address: Chemistry Department, University of Sofia, Bulgaria.

[1]J. Wintterlin, H. Brune, H. Höfer, and R. J. Behm, Appl. Phys. A **47**, 99 (1988); H. Brune, J. Wintterlin, G. Ertl, and R. J. Behm, Europhys. Lett. **13**, 123 (1990); E. Kopatzki and R. J. Behm, Surf. Sci. **245**, 255 (1991); R. Schuster, J. V. Barth, G. Ertl, and R. J. Behm, Phys. Rev. B **44**, 13 689 (1992).

[2]J. Tersoff and D. R. Hamann, Phys. Rev. Lett. **50**, 1998 (1983); Phys. Rev. B **31**, 805 (1985).

[3]A. A. Lucas, H. Morawitz, G. R. Henry, J.-P. Vigneron, Ph. Lambin, P. H. Cutler, and T. W. Feuchtwang, Solid State Commun. **65**, 1291 (1988).

[4]A. A. Lucas, H. Morawitz, G. R. Henry, J.-P. Vigneron, Ph. Lambin, P. H. Cutler, and T. E. Feuchtwang, Phys. Rev. B **37**, 10 708 (1988).

[5]G. Doyen, E. Koetter, J. Barth, and D. Drakova, in *Basic Concepts and Applications of Scanning Tunneling Microscopy (STM) and Related Techniques,* edited by R. J. Behm, N. Garcia, and H. Rohrer (Kluwer Academic, New York, 1990), p. 97.

[6]J. P. Vigneron, M. Scheffler, Th. Laloyaux, I. Derycke, and A. A. Lucas, Vacuum **41**, 745 (1990).

[7]J. B. Pendry, A. B. Prêtre, and B. C. H. Krutzen, J. Phys. Condens. Matter **3**, 4313 (1991).

[8]V. M. Hallmark, S. Chiang, J. F. Rabolt, J. D. Swalen, and R. J. Wilson, Phys. Rev. Lett. **59**, 2879 (1987).

[9]Ch. Wöll, S. Chiang, R. J. Wilson, and P. H. Lippel, Phys. Rev. B **39**, 7988 (1989).

[10]P. H. Lippel, R. J. Wilson, M. D. Miller, Ch. Wöll, and S. Chiang, Phys. Rev. Lett. **62**, 171 (1989).

[11]J. Wintterlin, J. Wiechers, H. Brune, T. Gritsch, H. Höfer, and R. J. Behm, Phys. Rev. Lett. **62**, 59 (1989).

[12]B. A. Lippmann, Phys. Rev. Lett. **15**, 11 (1965); **16**, 135 (1966).

[13]P. Ehrenfest, Z. Phys. **45**, 455 (1927).

[14]J. Bardeen, Phys. Rev. Lett. **6**, 57 (1961).

[15]G. Doyen, J. Phys. Condens. Matter (to be published).

[16]V. L. Moruzzi, J. F. Janak, and A. R. Williams, *Calculated Electronic Properties of Metals* (Pergamon, New York, 1978).

[17]K. Kambe and M. Scheffler, Surf. Sci. **89**, 262 (1979).

[18]F. Maca and M. Scheffler, Comput. Phys. Commun. **38**, 403 (1985); **52**, 381 (1988).

[19]S. Ciraci, A. Baratoff, and Inder P. Batra, Phys. Rev. B **41**, 2763 (1990).

[20]G. Doyen, E. Koetter, J. P. Vigneron, and M. Scheffler, Appl. Phys. A **51**, 281 (1990).

[21]J. Hölzl and F. K. Schulte, in *Solid Surface Physics,* edited by G. Höller, Springer Tracts in Modern Physics Vol. 85 (Springer, Berlin, 1979).

[22]H.-W. Fink, H. Schmid, H. J. Kreuzer, and A. Wierzbicki, Phys. Rev. Lett. **67**, 1543 (1991).

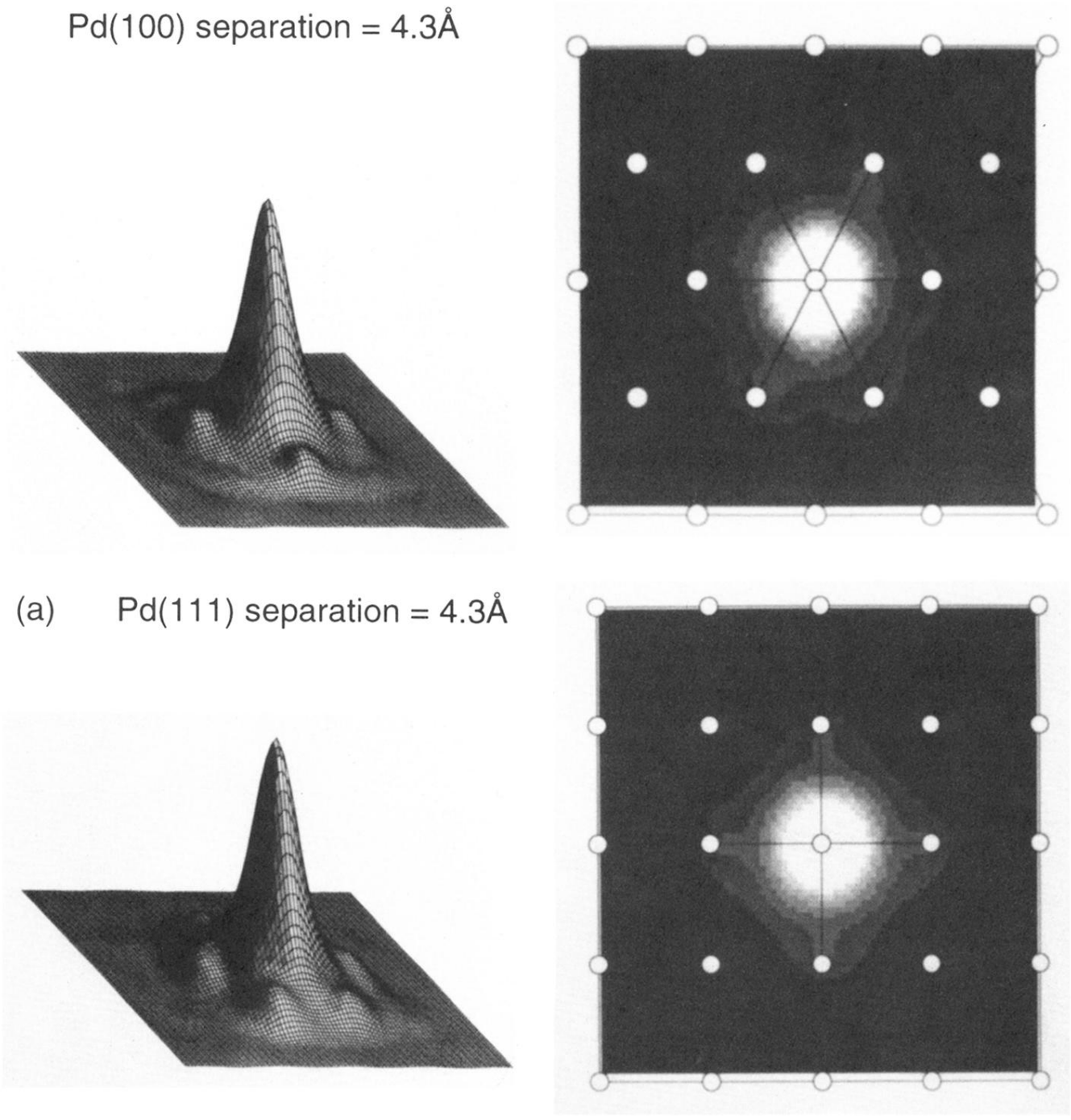

FIG. 10. 3D and Grey scale representation of the current density distribution parallel to the electrodes for the tip over a sample atom (tip-sample separation equal to 4.3 Å): (a) Pd(111) and Pd(100), (b) Al(111).

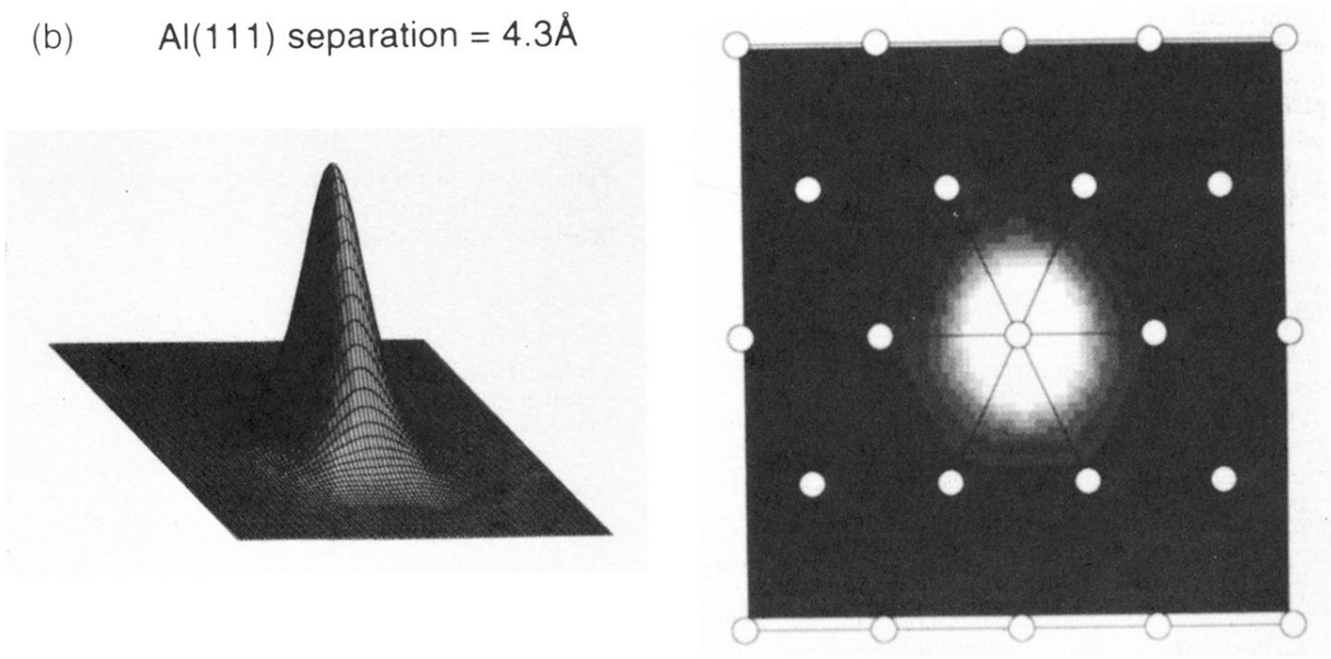

FIG. 10. (*Continued*).

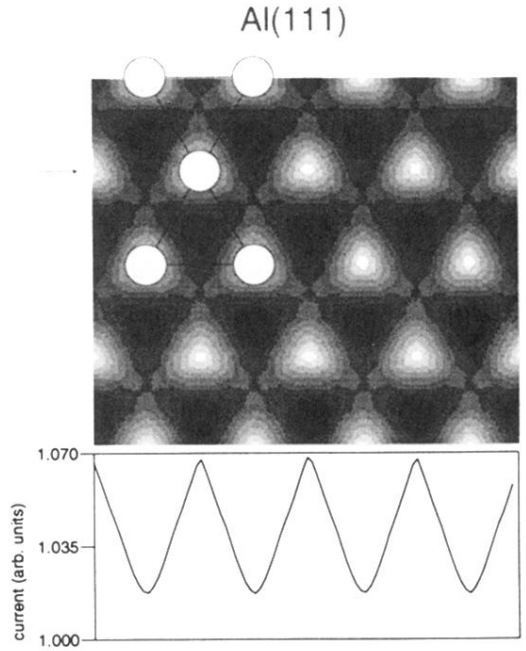

FIG. 2. Variation of the total tunnel current parallel to an Al(111) surface for a tip-sample separation of 3.5 Å. The maximal variation is 5.5%. The empty circles indicate Al atoms in the first layer.

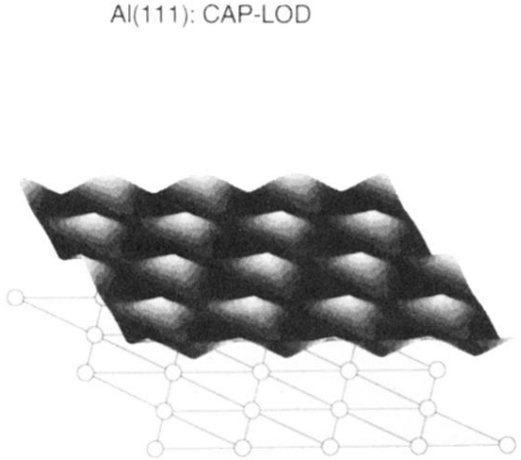

FIG. 4. Lateral variation of the capacitor projected local density at the Fermi level (CAP-LOD) [cf. Eq. (8)] for Al(111) at a tip-sample separation of 4.3 Å.

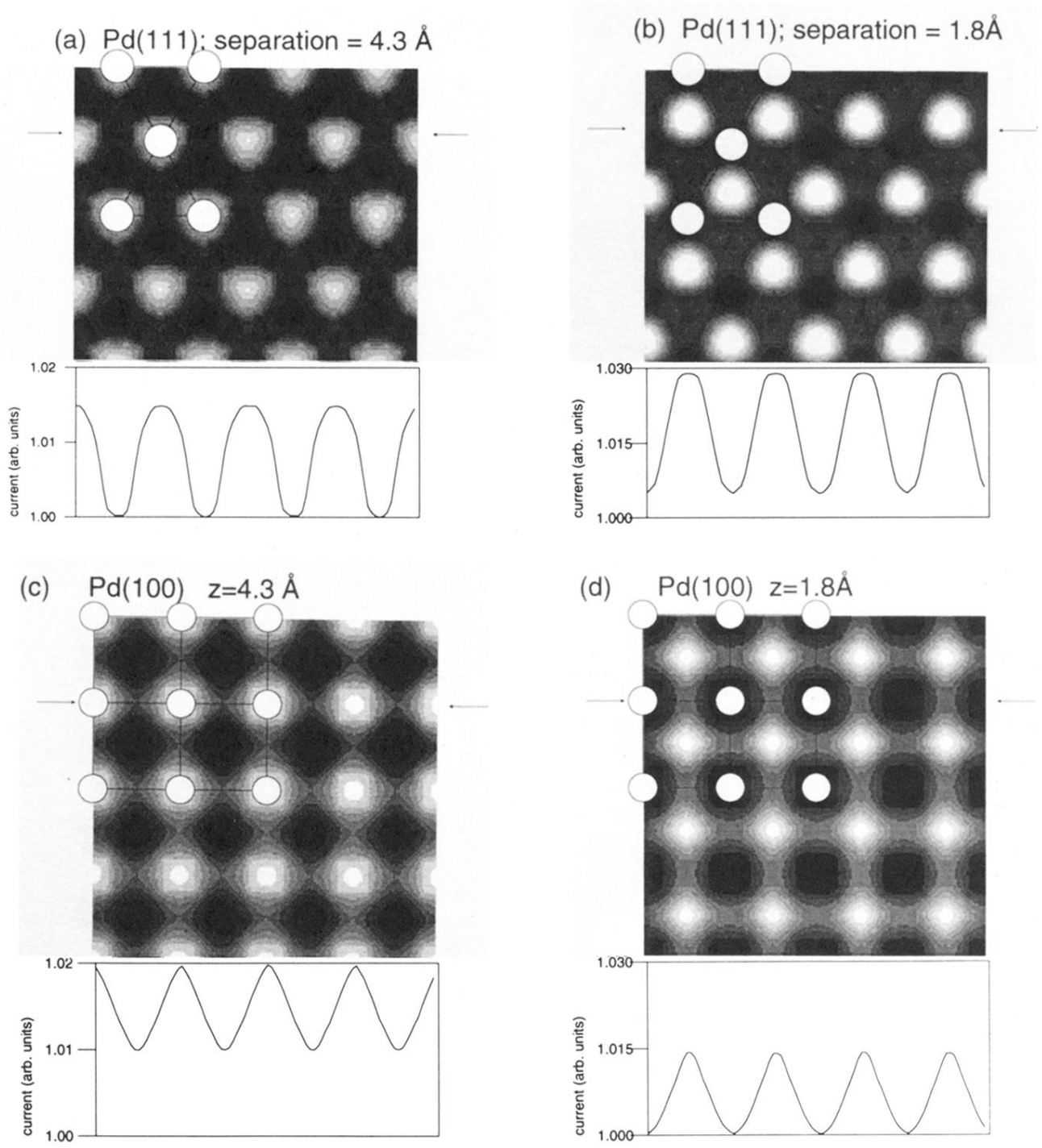

FIG. 5. Variation of the total tunnel current parallel to a Pd(111) and a Pd(100) surface at tip-sample separations of 4.3 [(a) and (c)] and 1.8 Å [(b) and (d)]. The open circles indicate the positions of the Pd atoms in the first layer.

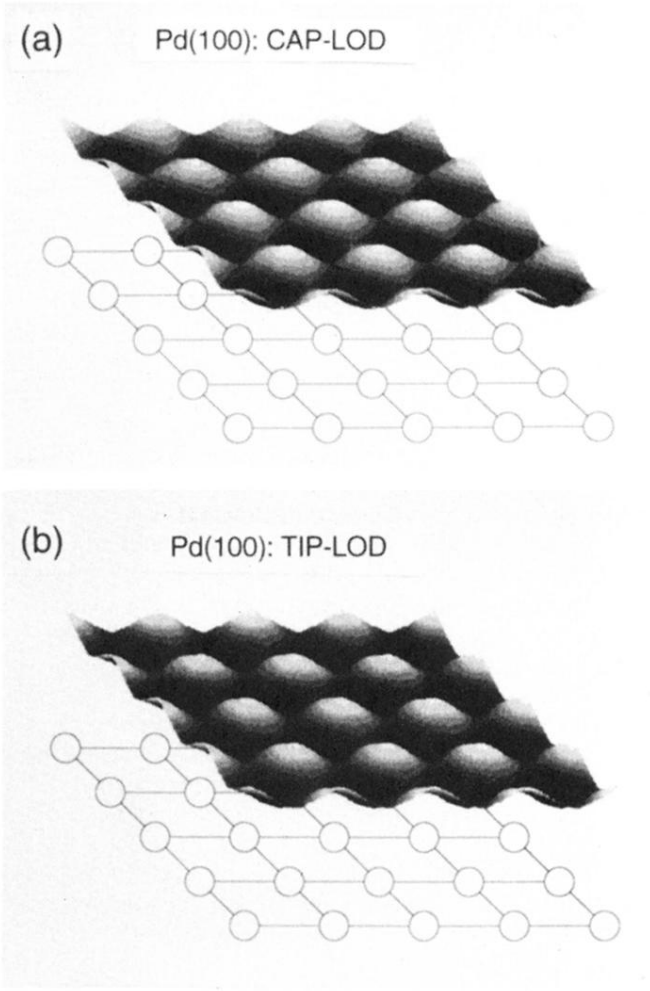

FIG. 6. Lateral variation of CAP-LOD (a) and TIP-LOD (b) for Pd(100) [cf. Eqs. (8) and (9)] for a tip-sample separation of 4.3 Å.

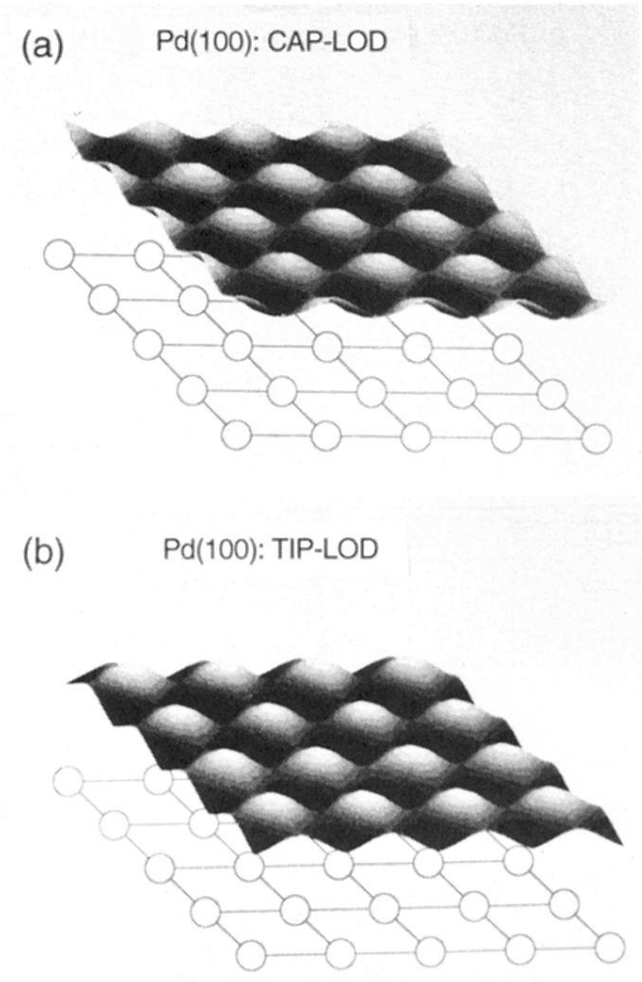

FIG. 7. Lateral variation of CAP-LOD (a) and TIP-LOD (b) for Pd(100) [cf. Eqs. (8) and (9)] for a tip-sample separation of 1.8 Å.

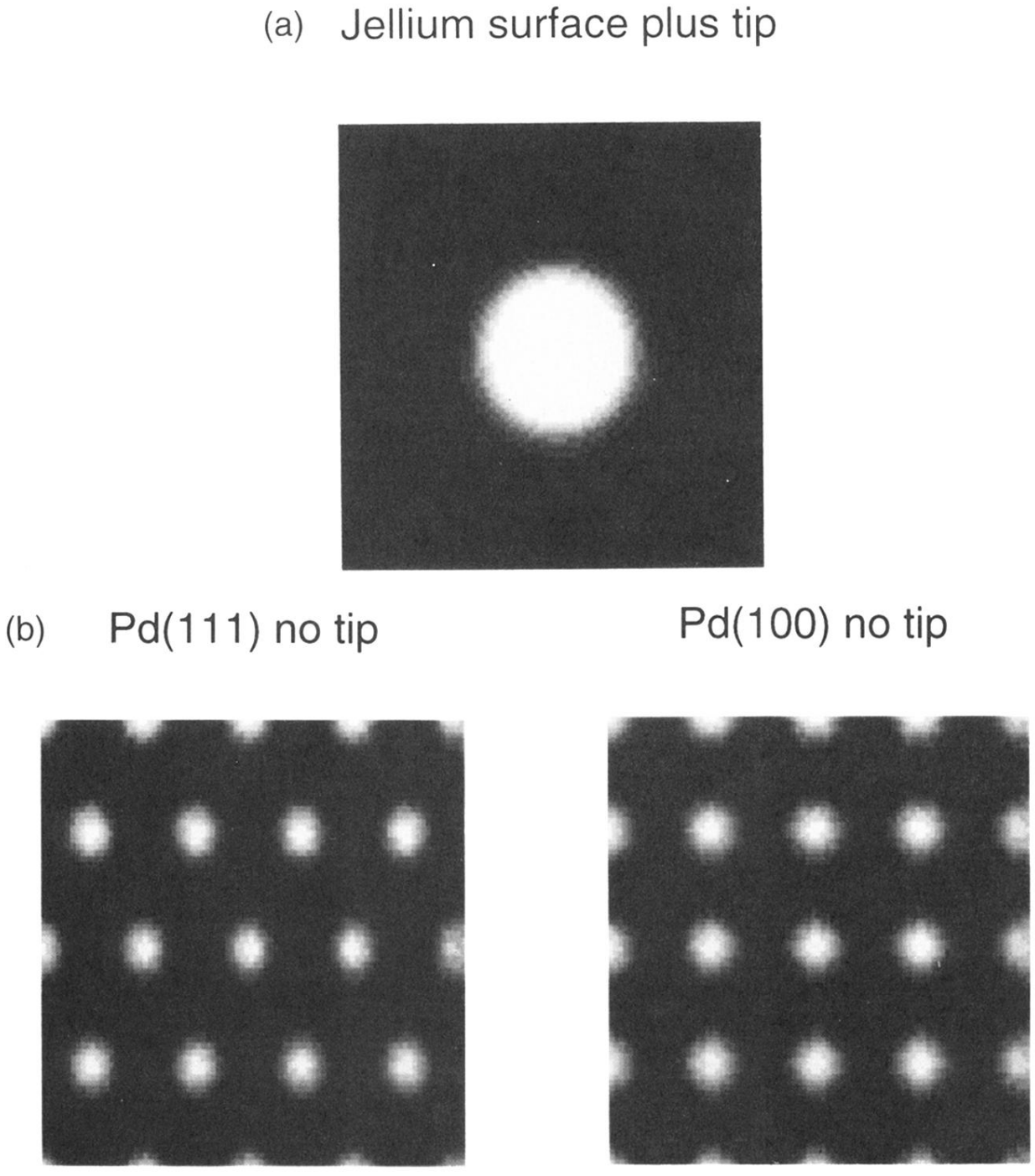

FIG. 9. Current densities for (a) tip with a structureless sample, (b) two electrode system (capacitor without tip) with Pd(100) and Pd(111) surfaces. The barrier width is the same in both cases (4.1 Å).